Wireless Personal Communications (2024) 136:1283–1296
https://doi.org/10.1007/s11277-024-11345-3

A Compact Half-Mode Substrate Integrated Waveguide Based Dual-Wideband Antenna

Meha Agrawal[1] · Trivesh Kumar[1] · Kapil Saraswat[2]

Accepted: 7 June 2024 / Published online: 20 June 2024

Abstract
A dual-wide-band triple resonance half mode substrate integrated waveguide (HMSIW) cavity-backed antenna with an extra shorting via is presented in this paper. Three modes of the HMSIW cavity are utilized to generate the dual-wide-band resonances. The HMSIW cavity along with three rectangular slots is fed coaxially which helps in achieving triple resonance and size miniaturization. An additional shorting via is loaded at the position of electric null between the 2nd and 3rd modes to bring the modes closer and couple them. The antenna exhibits one narrow band and one wide-band response. The dual-wide-band antenna is fabricated and tested on a low-profile substrate of 0.05 λ_g. A relative bandwidth of 1.03% (10.58–10.69 GHz) and 6.12% (12.47–13.25 GHz) is attained by the two bands. A stable broadside and unidirectional radiation pattern is achieved with a peak gain of 4.5 dBi, 5.81 dBi, and 6.18 dBi at 10.6 GHz, 12.68 GHz, and 13.2 GHz, respectively. Thus, the proposed dual-wide-band antenna can be effectively utilized for satellite applications.

Keywords Dual-band antenna · SIW · Wideband antenna

1 Introduction

Modern satellite antennas are growing more versatile and adaptable in order to withstand the challenging radio communication scenario. A dual-band antenna for dual applications in place of multiple antennas for multiple applications serves as a potential candidate for the development of compact, low-cost, and highly efficient satellite communication systems [1]. Dual-band responses can be obtained by exciting various cavity modes. Multiple slot radiators can be utilized to excite various cavity modes but the use of multiple slots increases the overall size of the antenna [2, 3]. These traditional multiband antennas continue to have limited overall bandwidth and poor gain [4]. Additionally, it is challenging to

✉ Trivesh Kumar
trivesh@iiitdmj.ac.in

1 Department of Electronics and Communication, Indian Institute of Information Technology, Design and Manufacturing, Jabalpur, India

2 Department of Electronics and Communication Engineering, Central University of Rajasthan, Ajmer, Rajasthan 305817, India

combine these antennas with radio-frequency (RF)-front end devices such that interference does not occur.

The recent development of substrate integrated waveguide (SIW) technology aids in the resolution of all the significant issues that plagued traditional microstrip antennas. SIW-based antennas offer remarkable qualities such as low-profile, lightweight, inexpensive fabrication, and simple planar technology integration [5]. Several SIW-based dual-band antennas are available in the literature. In [6], two triangular ring-shaped slot radiators are loaded in a square SIW cavity to achieve the dual-band response. In [7], a bow- tie-shaped slot is loaded in the SIW cavity to design a dual-band antenna. A circular ring-shaped slot-loaded structure also exhibits dual-frequency characteristics [8]. In [9], a square ring-shaped slot is etched on the top layer of the SIW cavity to get the dual-band responses. In [10], an E-shaped patch is loaded in a diamond-shaped SIW cavity to exhibit multiband characteristics. The SIW-based antennas have an important advantage of size miniaturization. The SIW structures may be divided in half, resulting in a size reduction of almost 50% while keeping the original SIW structure's performance attributes [11]. The ratio of substrate thickness to waveguide width always remains low which makes the SIW a planar version of the rectangular waveguide. Various HMSIW-based antennas are designed in literature by utilizing multiple rectangular slots, semi-circular slots, and the U-shaped slots [12–16]. However, all these HMSIW-based dual-band antennas exhibit narrow bandwidth.

In this paper, a new kind of dual-band cavity-backed antenna based on HMSIW is presented for satellite communication applications. Three rectangular slots are loaded in the half-SIW cavity to exhibit dual wideband response. Among three rectangular slots, two are tilted to exhibit lower frequency and contribute to further size miniaturization. Due to half-mode SIW arrangement and inclusion of slots results in a compact antenna. An extra shorting via is introduced at the position of the electric null to couple the two modes together for a wideband response. Thus, dual-band responses are obtained with both the two bands exhibiting narrow and wideband responses, respectively.

2 Antenna Design and Analysis

2.1 Proposed Antenna Configuration

The design configuration of the proposed compact dual-wideband antenna with the optimized dimensions is depicted in Fig. 1. The antenna is fed from the bottom side of the substrate by a 50 Ω coaxial feedline. The dual-band response is obtained by loading the HMSIW with three rectangular-shaped slots. The orientation of the two rectangular slots is altered to enhance the impedance matching and to accommodate longer-length slots in small size cavity. A shorting via is introduced to bring the two modes together and contribute to the attainment of wide-band response. X-band are used for the satellite communication because this band is resistance to atmospheric interference. Therefore, the HMSIW cavity dimensions are chosen such that the proposed antenna operates in X-band. A low loss dielectric substrate RT/Duroid 4003C with dielectric 3.55, loss tangent 0.0027, and thickness 1.57 mm is utilized for designing and fabricating the antenna. All the performance characteristics of the antennas are analyzed and obtained from the design and simulation software computer simulation technology (CST).

The dimensions of the SIW cavity are optimized to excite TE_{120} mode in the X-band and validated using the eigen-mode analysis in commercially available EM simulation software

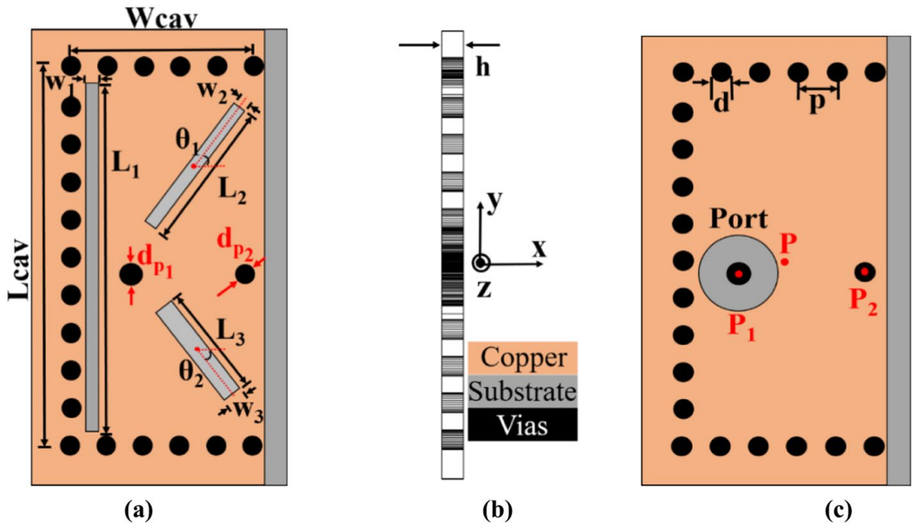

Fig. 1 Antenna design Configuration **a** top view, **b** side view, and **c** back view

(CST Studio Suite). The optimum dimensions of the SIW cavity dimensions are obtained using following equation [17–19]:

$$f_c = \frac{c}{2\sqrt{\varepsilon_r}}\sqrt{\left(\frac{m}{L_{cav}}\right)^2 + \left(\frac{n}{W_{cav}}\right)^2} \tag{1}$$

where, m and n are mode constants, 'L_{cav}' is the length SIW cavity (including the edge radius of SIW via) and 'W_{cav}' is width of the SIW cavity (including the edge radius of SIW via). To maintain minimum leakage losses, diameter of via and periodicity is chosen such that $p/d \leq 2$. The antenna dimensions are: $L_{cav}=20$, $W_{cav}=10$, $L_1=19$, $w_1=0.4$, $L_2=8.0$, $w_2=0.8$, $L_3=6.0$, $w_3=1.0$, $\theta_1=53°$, $\theta_2=-53°$, $h=1.57$, $d=1.0$, $p=2.0$, $dp_1=1.2$, $dp_2=1.0$, $P=(0,0)$, $P_1=(-1.8,-1.0)$, $P_2=(4.8,-1.0)$ All values are in 'mm'.

2.2 Design Methodology

The design evolution of the proposed antenna is depicted in Fig. 2. In step 1 the HMSIW cavity is excited by a 50 Ω coaxial probe. The real part of input impedance and S_{11} graphs of the design evolution can be distinguished from Fig. 3. Three individual modes at 12.07 GHz, 12.8 GHz, and 13.4 GHz are observed on exciting the HMSIW cavity. Although HMSIW cavity-based antennas provide size miniaturization but still in order to downscale the size, additional capacitance must be introduced. Therefore, in step 2, a rectangular slot of length L_1 and width w_1 is etched on the top layer of the HMSIW cavity. As an effect, the three original modes are shifted to 11.2 GHz, 12.7 GHz, and 13.3 GHz. To further downscale the size of the antenna, in step 3 another tilted rectangular slot of length L_2 and width w_2 is loaded on the same side of the cavity. As a result, all three modes are shifted to 10.6 GHz, 12.4 GHz, and 13.2 GHz. In step 4 one more tilted rectangular slot of length L_3 and width w_3 is loaded and the three modes are

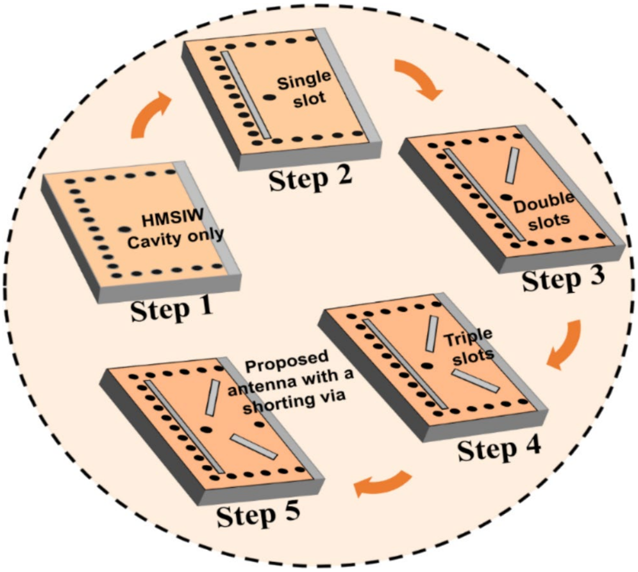

Fig. 2 Step-by-step design evolution of the dual-wideband antenna

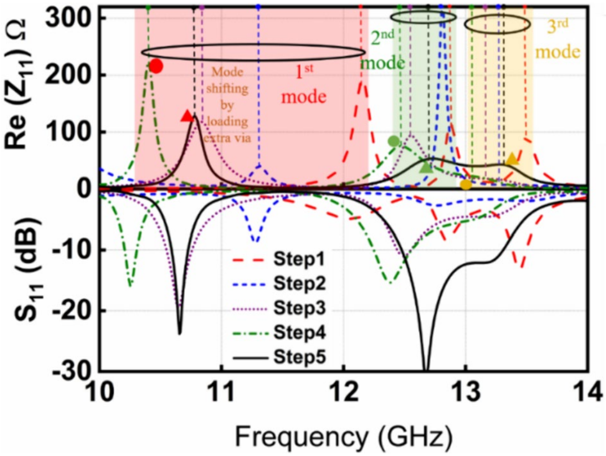

Fig. 3 Real part of input impedance and reflection coefficient of the design evolution

further shifted to 10.2 GHz, 12.3 GHz, and 13.02 GHz. Similar shifting in resonances is observed. The S_{11} plot of step 4 shows a dual narrow-band response. Therefore, in order to enhance the bandwidth of the dual narrow bands, the 2nd mode and 3rd mode can be coupled together. However, since the 1st mode is far away from the 2nd mode, therefore it cannot be coupled with other modes. Thus, in step 5 a shorting via is loaded inside the HMSIW cavity. The shorting via is aligned with the feed and placed at the null point of the 2nd mode and third mode to yield maximum impedance matching. It can be observed that the 2nd mode and the 3rd mode are coupled together to exhibit a dual wide-band response. Thus, the extra shorting via enhances the impedance matching,

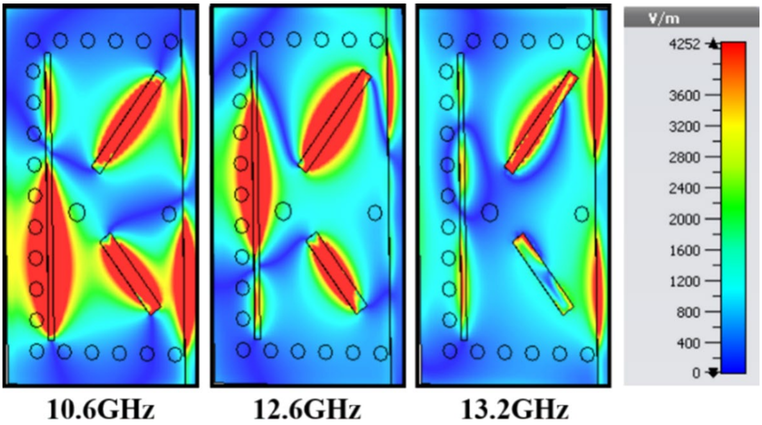

Fig. 4 Electric-filed distribution of the HMSIW based antenna at the three resonant frequencies

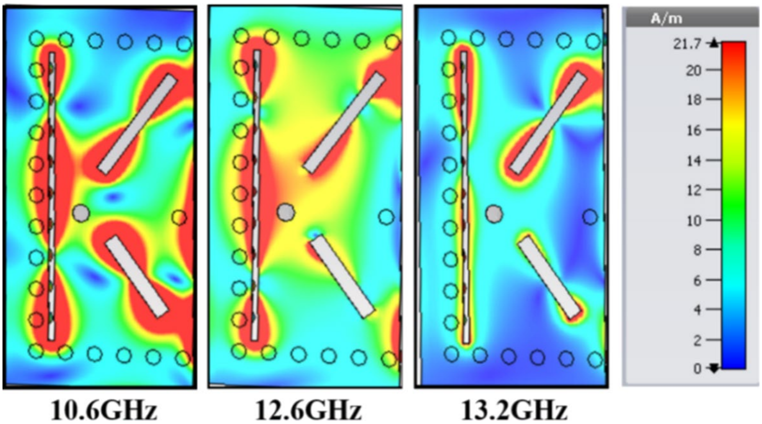

Fig. 5 Surface-current distribution of the HMSIW based antenna at the three resonant frequencies

coupled the two modes, and also greatly perturbs all three modes thereby shifting them towards the higher frequency regime at 10.6 GHz, 12.68 GHz, and 13.2 GHz.

2.3 Electric-Field Distribution

The electric-field distribution and the surface current distribution of the via-loaded dual wideband antenna at three frequencies are shown in Figs. 4 and 5 respectively. It can be observed that as the 1st slot is having minimum electric field strength at the extreme ends at 12.68 GHz and 13.2 GHz, hence it does not affect the two resonances. However, the other two slots affect all three resonances. It can also be observed that the smallest current path contributes to the highest frequency 13.2 GHz and the longest current path contributes to the lowest frequency 10.6 GHz.

2.4 Equivalent Circuit Model of Proposed HMSIW Antenna

The proposed antenna design is further analysed by developing an equivalent circuit model portrayed in Fig. 6a. The three modes existing inside the HMSIW cavity are modelled by the parallel RLC circuit components $PRLC_n$ (where n = 1, 2, 3, 4). The coaxial feed is coupled to the HMSIW cavity by the transformer T_1. The loading effect in HMSIW cavity is introduced by the series capacitor and inductor Cs Ls. The three radiating slots are modelled together by series arrangement of R_{RE} L_{RE} C_{RE}. These radiating slots are coupled to the SIW cavity by the transformer T_2. The effect of extra via is modelled by the parallel RLC component PRLCv. The coaxial feed line is modelled by the resistor RF. The circuit is designed and simulated by using pathwave advanced design system (ADS) software to obtain the finally optimized values of circuit components: $R_F = 1.2\ \Omega$, $T_1 = T_2 = 1.79$, $PRLC_1 = (7.5\ K\Omega, 0.165\ nH, 0.752\ pF)$, $PRLC_2 = (0.7\ K\Omega, 0.522\ nH, 0.568\ pF)$, $PRLC_3 = (5.78\ K\Omega, 0.112\ nH, 1.196\ pF)$, $PRLC_4 = (6.1\ K\Omega, 0.210\ nH, 0.714\ pF)$, Cs = 3.26 pF, Ls = 0.296 nH, PRLCv = (11.25 Ω, 1.31 nH, 0.5 pF), Cs = 1.31 pF, $R_{RE} = 250\Omega$, $L_{RE} = 4.325nH$, $C_{RE} = 0.5pF$. The response obtained by simulating the equivalent circuit model is compared with the response obtained from CST software. The reflection coefficient obtained from the equivalent circuit model agree with the result obtained from the full wave EM simulation and shown in Fig. 6b. The root mean square error for Fig. 6b is calculated to be 7.96%.

2.5 Parametric Variation

The resonant frequencies of both the bands are dependent on the length of the three slots and their tilt angle. Figure 7 shows the effect of variation of dimensional parameters on the dual-band response. The effect of variation of the 1st slot length is shown in Fig. 7a. It is observed that on increasing the slot length the resonance frequency 10.6 GHz shifts towards the lower frequency regime because the effective capacitance of the HMSIW cavity increases. A similar effect of variation is also modeled by an equivalent circuit and shown in Table 1. The variation in the width of the 1st slot shown in Fig. 7b introduces a small variation in the current path changes the effective length of an antenna and thereby slightly affecting the lower resonance [20–23]. Table 2 depicts

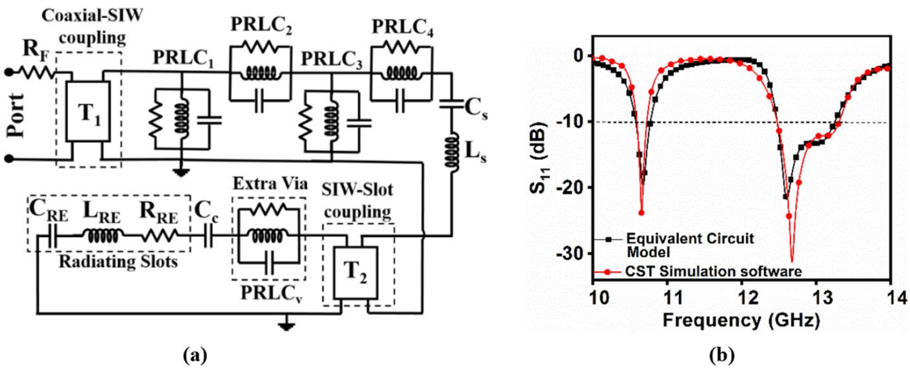

Fig. 6 Comparison between reflection coefficient (S_{11}) obtained using **a** Equivalent circuit model, and **b** full wave EM simulation (CST studio suite)

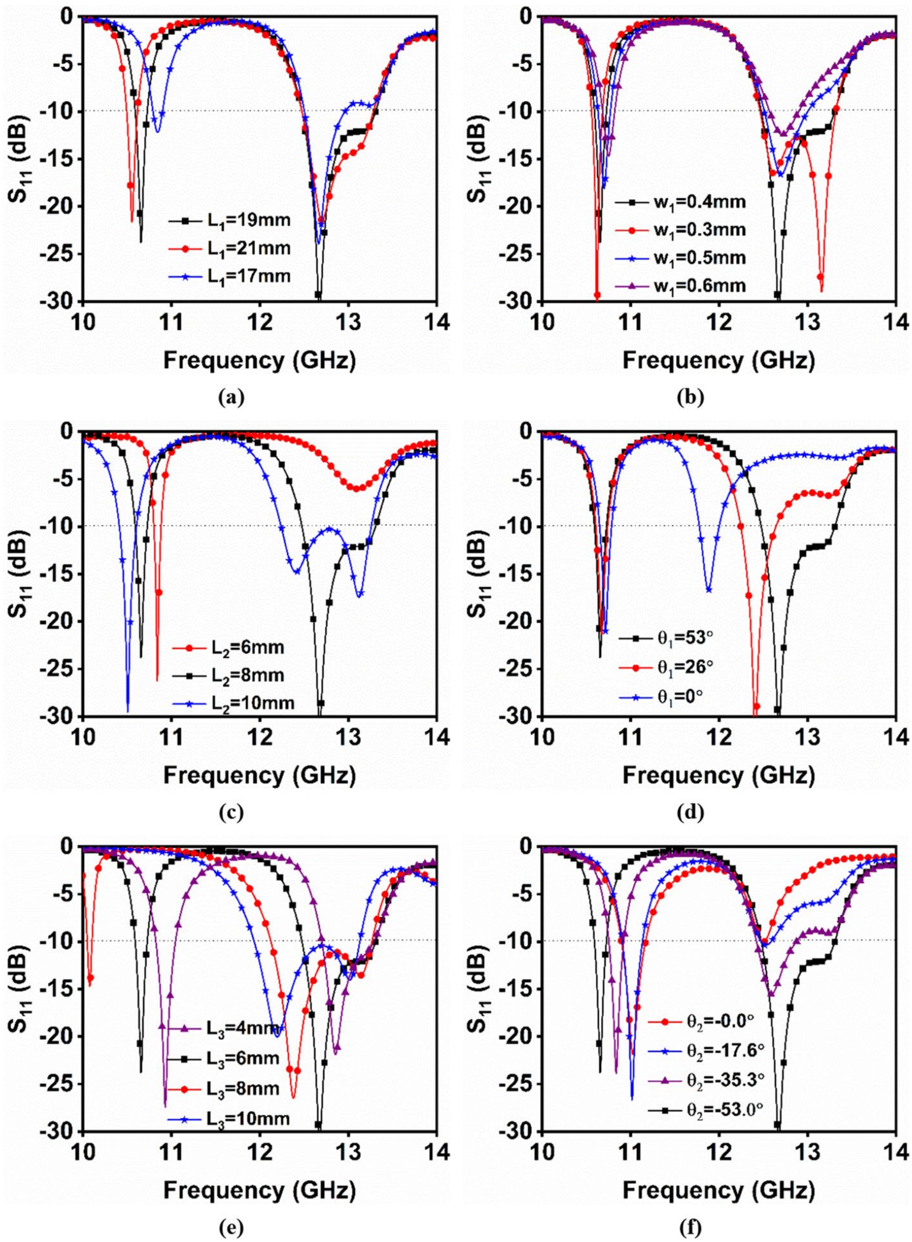

Fig. 7 Effect of parametric variation on the antenna performance

the equivalent change in the circuit components. Further, on increasing the length of the 2nd slot the first two resonance frequencies 10.6 GHz and 12.68 GHz are shifted to the lower frequency side (Fig. 7c). However, the third resonance frequency is very slightly affected. It can be observed that at $L_2 = 10$ mm the coupling of the 2nd mode and the 3rd mode is achieved at an earlier stage as compared to that at $L_2 = 8$ mm. A larger

Table 1 Effect of variation of slot length L_1

Resonant frequency (GHz)	Circuit model		Geometrical parameter L_1 (mm)
	$C_2 = 0.568$ pF (Fixed)	$L_2 = 0.522$ nH (Fixed)	
	L_2 (nH)	C_2 (pF)	
10.75	0.493	0.550	17
10.60	0.522	0.568	19
10.50	0.613	0.608	21

Table 2 Effect of variation of width of 1st rectangular slot

Resonant frequency (GHz)	Circuit model		Geometrical parameter w_1 (mm)
	$C_3 = 1.196$ pF (Fixed)	$L_3 = 0.112$ nH (Fixed)	
	L_3 (nH)	C_3 (pF)	
10.55, 12.55	0.129	1.312	0.3
10.60, 12.60	0.112	1.196	0.4
10.65, 12.65	0.100	1.182	0.5
10.70, 12.70	0.878	0.964	0.6

Table 3 Effect of variation of length of rectangular slot L_2

Resonant frequency (GHz)	Circuit model		Geometrical parameter L_2 (mm)
	$C_1 = 0.752$ pF (Fixed)	$L_1 = 0.165$ nH (Fixed)	
	L_1 (nH)	C_1 (pF)	
10.85	0.194	0.543	6
10.60	0.165	0.752	8
10.45	0.148	0.938	10

bandwidth is observed at $L_2 = 10$ mm but a small fabrication ambiguity may result in loss of mode coupling. Therefore, $L_2 = 8$ mm is considered to be the most optimum length of the 2nd slot. Table 3 shows the equivalent effect on circuit components.

The variation of the tilt angle of the 2nd slot is shown in Fig. 7d. An increase in tilt angle increases the gap between the 1st and 2nd slots. The 2nd resonance frequency shifts towards the 3rd resonance frequency thereby coupling the 2nd and 3rd modes. On increasing the tilt angle beyond 53°, the 2nd resonance continues to shift but the bandwidth gets reduced. Therefore, tilt angle $\theta_2 = 53°$ is considered the most optimum value. It can also be observed that the 1st and 3rd resonance frequencies remain unaffected by varying the tilt angle θ_2. The effect of variation of the 3rd slot length is shown in Fig. 7e. On varying the 3rd slot length all three current paths are affected. Therefore, on increasing the length of the 3rd slot all three resonant frequencies are shifted towards the lower frequency regime. Table 4 shows the equivalent effect of variation of third slot length on the circuit components.

Table 4 Effect of variation of length of rectangular slot L_3

Resonant frequency (GHz)	Circuit model				Geometrical parameter L_3 (mm)
	$C_2=0.568$ pF (Fixed), $C_4=0.714$ pF (Fixed)		$L_2=0.522$ nH (Fixed), $L_4=0.210$ nH (Fixed)		
	L_2 (nH)	L_4 (nH)	C_2 (pF)	C_4 (pF)	
10.85, 12.85	0.501	0.205	0.541	0.684	4
10.60, 12.60	0.522	0.210	0.568	0.714	6
10.20, 12.30	0.650	0.326	0.660	0.896	8
9.95, 12.15	0.882	0.542	0.751	0.994	10

Further, on increasing the tilt angle of the 3rd slot in the clockwise direction (Fig. 7f), again the gap between the 1st slot and 3rd slot increases while the gap between the 2nd and 3rd slot decreases. Thus on increasing the tilt angle the 1st resonance shifts towards the lower frequency regime while the 2nd and 3rd resonances get closer to forming wide bandwidth.

Using the observations from the parametric studies, equivalent circuit model and initial design guidelines (as discussed in Sect. 2.1) the proposed antenna can be designed and optimized for any other frequency band.

3 Fabrication and Measurement

The proposed compact HMSIW dual-band cavity-backed antenna is fabricated on Rogers RT/Duroid 4003 substrate using milling machine (LPKF ProtoMat S103 rapid prototyping machine) because of effortless and precise fabrication of SIW via etc. The SMA connector is connected through the bottom of the substrate. The fabricated prototype antenna is tested using a vector network analyzer. The picture of the fabricated antenna is shown in Fig. 8a. A good agreement between the simulated and measured reflection coefficient can be observed in Fig. 8b. The measured S_{11} bandwidth (−10 dB) of the two bands is 10.58–10.69 GHz and 12.47–13.25 GHz. Table 5 depicts the performance comparison between measured and simulated results. A small variation in the measured and simulated S_{11} responses can be due to fabrication ambiguities.

Further, the radiation pattern of the antenna is measured in an anechoic chamber. Figure 9 shows the measured and simulated radiation pattern at the three resonance frequencies in both XZ and YZ planes. A unidirectional radiation pattern (linearly polarized) is observed with the direction of broadside radiation along the +z axis. The level of cross-polarization at 10.6 GHz, 12.6 GHz, and 13.2 GHz is −10 dB, −18 dB, and −15 dB, respectively. The comparison between simulated and measured peak gain in the broadside direction is portrayed in Fig. 10. The measured peak gain in the band 10.5–10.7 GHz is observed to be greater than 4.2 dBi and in the band 12.4–13.4 GHz, it is greater than 5.5 dBi. However, the peak gain observed at 10.6 GHz, 12.6 GHz, and 13.2 GHz is 4.5 dBi, 5.81 dBi, and 6.18 dBi, respectively.

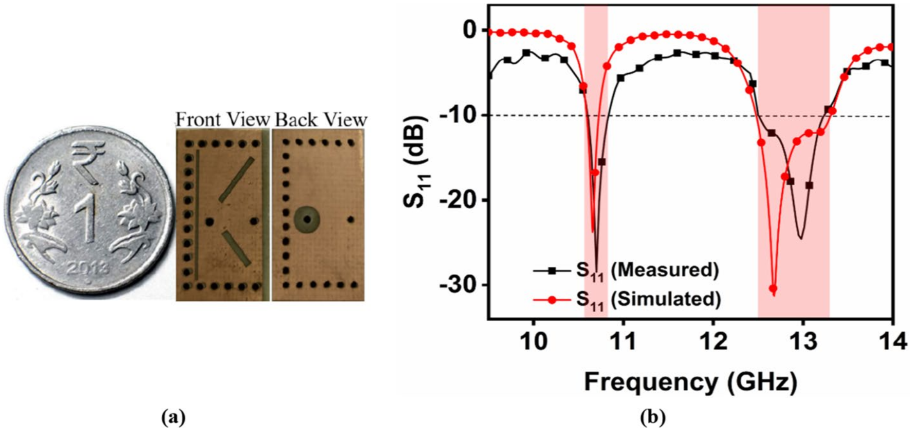

Fig. 8 **a** Photograph of the fabricated antenna, **b** Comparison between simulated S_{11} and measured S_{11} of proposed HMSIW dual-wideband antenna

Table 5 Comparison between measured and simulated performance of dual wideband antenna

Band	Freq. Bands	f_c (GHz)	BW (%)	Gain (dBi)	X-pol (dB)
1	10.58–10.73 GHz (Sim.)	10.60	1.4	4.7	− 9.5
	10.58–10.69 GHz (Mea.)	10.58	1.03	4.5	− 10
2	12.47–13.30 GHz (Sim.)	12.68, 13.2	6.5	6.0, 6.8	− 19, − 15
	12.47–13.25 GHz (Mea.)	12.67, 13.15	6.12	5.81, 6.18	− 18, − 15

A performance comparison of the proposed antenna with other previously reported similar works is presented in Table 6. Thus, from the comparison table, it can be inferred that the proposed dual-band antenna exhibits wide bandwidth by coupling the 2nd and 3rd modes through a shorting via. Also, the antenna is compact in size with a considerable amount of peak gain in both bands.

4 Conclusion

A coaxially fed dual-wideband antenna has been presented by loading three rectangular slots in an HMSIW cavity. The advantages of the HMSIW cavity with a shorting via are utilized to design the proposed dual-wideband antenna. The designed antenna provides the promising performance with the following benefits: (1) A compact size low profile antenna with a simple feeding mechanism; (2) a unidirectional and stable radiation pattern in the broadside direction; (3) wider bandwidth; (4) acceptable level of gain and low cross-polarization. Additionally, the proposed antenna is also modelled with the equivalent circuit with detailed parametric values. The proposed compact HWSIW dual wideband antenna is therefore a good alternative for contemporary satellite communication applications.

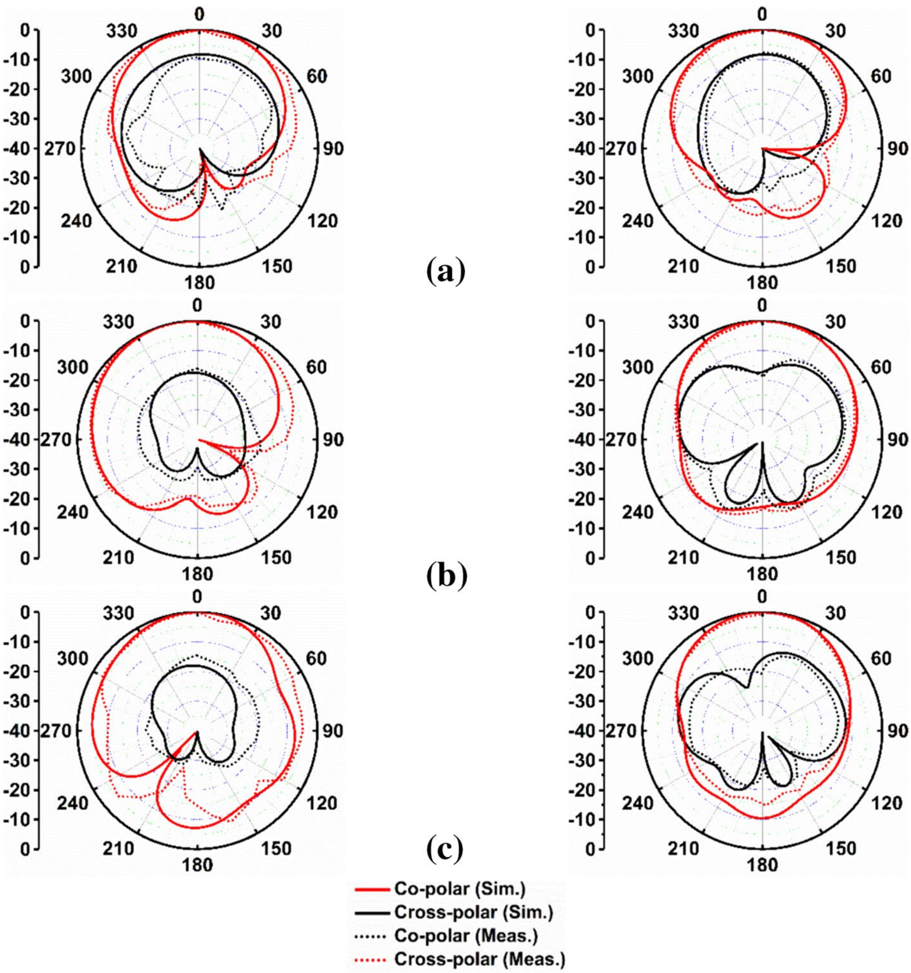

Fig. 9 Simulated and measured radiation patterns at **a** 10.6 GHz, **b** 12.68 GHz, and **c** 13.2 GHz

Fig. 10 Peak gain of the antenna in the dual-bands

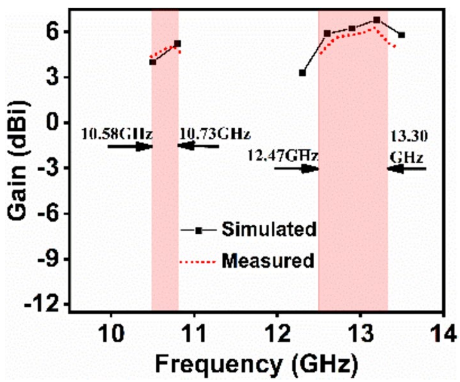

Table 6 Performance comparison of proposed HMSIW-based dual wideband antenna with other reported works

References	Freq. (GHz)	BW (%)	Gain (dBi)	Cavity size (λ_g^2)
[1]	9.7, 14.85	6.1, 4.7	12.8, 13.5	4.6 × 1.3
[6]	8.6, 13.43	2.3, 6.02	5.1, 6.3	0.85 × 0.73
[7]	10.33, 11.8	4.9, 7.1	5.23, 4.3	1.08 × 0.74
[8]	37.45, 47.9	1.06, 1.35	5, 5.7	1.64 × 0.99
[9]	13.4,17.9	1.1, 2	13.4	0.89 × 0.89
[12]	4.6, 5.4	2.1, 1.8	5.1, 5.5	0.75 × 0.51
[13]	5.0, 5.75	3.0, 3.1	6.25, 6.0	1.09 × 0.82
[14]	8.5, 10.6	2.75, 3.42	7.5, 6.0	0.83 × 0.47
[15]	8.8, 11.3	2.0, 1.4	5.3, 4.3	0.65 × 0.60
[16]	5.75, 9.56	0.94, 0.62	4.9, 5.7	1.05 × 1.05
This work	10.6, 12.84	1.03, 6.12	4.5, 6.18	0.35 × 0.70

Funding No funding was received for conducting this research.

Data Availability Data sharing not applicable to this article as no datasets were generated or analysed during the current study.

Declarations

Conflict of interest The author declares no potential conflict of interest.

References

1. Wei, D.-J., Li, J., Yang, G., Liu, J., & Yang, J.-J. (2018). Design of compact dual-band SIW slotted array antenna. *IEEE Antennas and Wireless Propagation Letters, 17*(6), 1085–1089.
2. Wang, Y.-S., Lee, M.-C., & Chung, S.-J. (2007). Two PIFA-related miniaturized dual-band antennas. *IEEE Transactions on Antennas and Propagation, 55*(3), 805–811.
3. Lee, C.-T., & Wong, K.-L. (2009). Uniplanar printed coupled-fed PIFA with a band-notching slit for WLAN/WiMAX operation in the laptop computer. *IEEE Transactions on Antennas and Propagation, 57*(4), 1252–1258.
4. Mukherjee, S., Biswas, A., & Srivastava, K. V. (2014). Broadband substrate integrated waveguide cavity-backed bow-tie slot antenna. *IEEE Antennas and Wireless Propagation Letters, 13*, 1152–1155.
5. Bozzi, M., Georgiadis, A., & Wu, K. (2011). Review of substrate-integrated waveguide circuits and antennas. *IET Microwaves, Antennas & Propagation, 5*(8), 909–920.
6. Kumar, A., Saravanakumar, M., & Raghavan, S. (2018). Dual-frequency SIW-based cavity-backed antenna. *AEU-International Journal of Electronics and Communications, 97*, 195–201.
7. Nandi, S., & Mohan, A. (2016). Bowtie slotted dual-band SIW antenna. *Microwave and Optical Technology Letters, 58*(10), 2303–2308.
8. Wu, Q., Yin, J., Yu, C., Wang, H., & Hong, W. (2017). Low-profile millimeter-wave SIW cavity-backed dual-band circularly polarized antenna. *IEEE Transactions on Antennas and Propagation, 65*(12), 7310–7315.
9. Lee, H., Sung, Y., Wu, C.-T.M., & Itoh, T. (2015). Dual-band and polarization-flexible cavity antenna based on substrate integrated waveguide. *IEEE Antennas and Wireless Propagation Letters, 15*, 488–491.
10. Agrawal, M., & Kumar, T. (2021a). A multiband E-shaped substrate integrated waveguide-based antenna for X, Ku K-band applications. *IETE Journal of Research, 69*(9), 5898–5908.
11. Agrawal, M., & Kumar, T. (2021b). Half substrate integrated waveguide based wideband slot antenna. In *2021 IEEE 18th India council international conference (INDICON)* (pp. 1–5).

12. Yang, X., Ge, L., Ji, Y., Zeng, X., & Luk, K. M. (2019). Design of low-profile multi-band half-mode substrate-integrated waveguide antennas. *IEEE Transactions on Antennas and Propagation, 67*(10), 6639–6644.
13. Chaturvedi, D., & Raghavan, S. (2018). A dual-band half-mode substrate integrated waveguide-based antenna for WLAN/WBAN applications. *International Journal of RF and Microwave Computer-Aided Engineering, 28*(5), e21239.
14. Jagadeesh, D., & Sudhakar, A. (2019). Dual band half mode SIW semi circular cavity back slot antenna. *Progress In Electromagnetics Research Letters, 87*, 7–14.
15. Althuwayb, A. A., Al-Hasan, M. J., Kumar, A., & Chaturvedi, D. (2021). Design of half-mode substrate integrated cavity inspired dual-band antenna. *International Journal of RF and Microwave Computer-Aided Engineering, 31*(2), e22520.
16. Banerjee, S., Rana, B., & Parui, S. K. (2016). SIW based compact and dual-band equilateral triangular antennas. *Journal of Electromagnetic Waves and Applications, 30*(5), 637–650.
17. Deslandes, D., & Wu, K. (2006). Accurate modeling, wave mechanisms, and design considerations of a substrate integrated waveguide. *IEEE Transactions on Microwave Theory and Techniques, 54*(6), 2516–2526.
18. Xu, F., & Wu, K. (2005). Guided-wave and leakage characteristics of substrate integrated waveguide. *IEEE Transactions on Microwave Theory and Techniques, 53*(1), 66–73.
19. Lai, Q., Fumeaux, C., Hong, W., & Vahldieck, R. (2009). Characterization of the propagation properties of the half-mode substrate integrated waveguide. *IEEE Transactions on Microwave Theory and Techniques, 57*(8), 1996–2004.
20. Sran, S. S., & Sivia, J. S. (2023). Design of a novel wearable hybrid fractal antenna for Wi-Fi, bluetooth, and WiMax applications. *Wireless Personal Communications, 132*, 737–755.
21. Bhatia, S. S., Sivia, J. S., & Sarao, A. K. (2022). Lantern logo shaped novel monopole antenna with semi-circular notch loaded partial ground plane for ultra-wideband wireless applications. *Wireless Personal Communications, 126*, 3211–3231.
22. Bharti, G., & Sivia, J. S. (2022). A design of compact wideband antenna based on hybridization of Minkowski fractal curves on hexagonal patch and partial ground plane with truncated corners. *Wireless Personal Communications, 124*, 1609–1621.
23. Sran, S. S., & Sivia, J. S. (2020). ANN and IFS based wearable hybrid fractal antenna with DGS for S, C and X band application. *AEU—International Journal of Electronics and Communications, 127*, 153425.

Meha Agrawal received B.Tech and M.Tech degrees from U.P.T.U, Lucknow and N.I.T, Kurukshetra, India, respectively. She is presently a Research Scholar with the Microwave Communication Section, Indian Institute of Information Technology Design and Manufacturing, Jabalpur, India. Her research areas are the design of SIW based antennas.

Trivesh Kumar received his Ph.D. in Electrical engineering from Indian Institute of Technology Kanpur, India. He is presently an Assistant Professor in the Department of Electronics and Communication Engineering, Indian Institute of Information Technology, Design and Manufacturing, Jabalpur, India. The main areas of his research features circularly-polarized antennas and analysis, microwave-measurements, RFID, substrate integrated waveguide structures, and many more.

Kapil Saraswat is an Assistant Professor at the Central University of Rajasthan, affiliated with the Department of Electronics and Communication Engineering. He received his M. Tech. degree from Indian Institute of Technology Roorkee in electronics and communication engineering, and the Ph.D. degree from Indian Institute of Technology Kanpur in 2019 in electrical engineering. His current research activities include CP antennas, reconfigurable antennas, computational electromagnetics, CM analysis, antenna measurement techniques etc.